Progress In Electromagnetics Research, Vol. 107, 63–99, 2010

SCATTERING OF ELECTROMAGNETIC WAVES FROM A RECTANGULAR PLATE USING AN EXTENDED STATIONARY PHASE METHOD BASED ON FRESNEL FUNCTIONS (SPM-F)

C. G. Moschovitis

Division of Information Transmission Systems and Materials Technology
School of Electrical and Computer Engineering
National Technical University of Athens
9 Iroon Polytechniou Str., Zografou, Athens GR-15780, Greece

H. T. Anastassiu

Hellenic Aerospace Industry
P. O. Box 23 GR-32009, Schimatari, Tanagra/Viotia, Greece

P. V. Frangos

Division of Information Transmission Systems and Materials Technology
School of Electrical and Computer Engineering
National Technical University of Athens
9 Iroon Polytechniou Str., Zografou, Athens GR-15780, Greece

Abstract—This paper presents an extension over a novel, three dimensional high frequency method for the calculation of the scattered electromagnetic (EM) field from a Perfect Electric Conductor (PEC) plate, which is based on the Physical Optics (PO) approximation and the Stationary Phase Method (SPM). This extension defines a new analytical method which is proved to be very efficient in computer execution time and enhances the accuracy of its predecessor around the area of the main scattering lobe. This new analytical method accomplishes high accuracy through the use of higher order approximation terms, which imply the use of Fresnel functions (SPM-F method). By using higher order Fresnel approximation terms, no impact on the time efficiency of the SPM method appears to

Received 1 April 2010, Accepted 20 July 2010, Scheduled 1 August 2010
Corresponding author: C. G. Moschovitis, (harism@noc.ntua.gr).

occur, since the extended SPM-F method just removes the troublesome vanishing denominators when the stationary point coincides with the edges of the scatterer. The SPM-F results are compared to other straightforward numerical and exact solution methods for the same problem in the far field, Fresnel zone and the near field area of the scatterer.

1. INTRODUCTION

In a recent publication [1], we have developed and presented a novel three-dimensional (3-D) high frequency analytical method for the calculation of the vector potential $\underline{A}$, and eventually the scattered electromagnetic field (EM) from a Perfect Electric Conductor (PEC) plate geometry, which is presented in Fig. 1. This method is based on Physical Optics (PO) approximation and Stationary Phase Method (SPM) three dimensional calculations. Comparisons with numerical integration end exact solution results yielded excellent agreement, except for the main scattering lobe. This discrepancy is due to the fact that the denominator of the first order analytical approximation vanishes when the stationary point coincides with the end point located at the edges of the scatterer, i.e., the rectangular plate. In this paper, we present a higher order approximation term for the edge contribution, which is based again on the Stationary Phase Method, but also includes Fresnel functions, hence the name (SPM-F). Using Fresnel functions, the accuracy is improved and the newly derived method lacks any singularities/inaccuracies in the vicinity of the main scattering lobe encountered in earlier published SPM results [1]. Vector potential $\underline{A}$ and scattered electric field $\underline{E}$ expressions are derived in the sections below, according to the modified version of the method that was presented in [1], but now all calculations include the new Fresnel terms. Fig. 1, below, shows the geometry of scattering of an electromagnetic (EM) wave with incident wavevector k_i from a perfect electric conductor (PEC) rectangular plate. The scattered field is calculated at an arbitrary observation point $R(x, y, z)$.

Possible applications of the extended 3D-SPM-F method include common radio-propagation tools in urban outdoor environment, where 2D [2] and 3D (under development by our research group) scattering and diffraction calculations take place, including both first and second order scattering phenomena. In such microcellular geometries in 2D [2], both transmitter and receiver are considered to be well below rooftop level and well above the ground. A 2-D approach leads to field calculation by calculating single integrals, while a 3-D approach — more complicated formulation presented in next sections

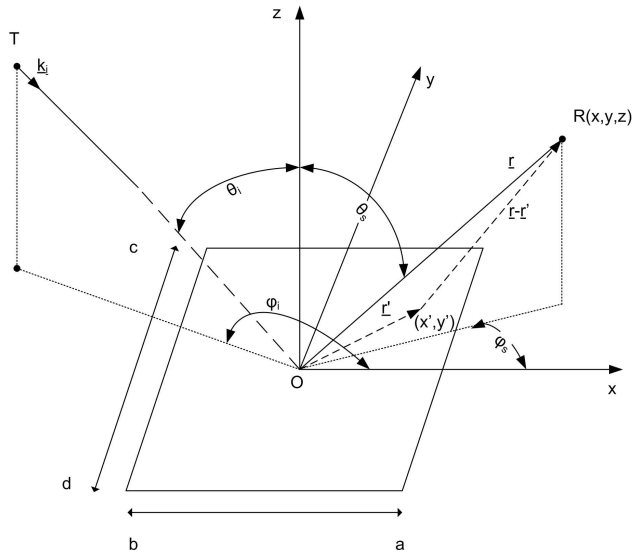

Figure 1. Scattering from a PEC rectangular plate of dimensions $a-b$ and $c-d$.

of this publication — requires the calculation of double integrals. Both single and double integral calculations may be achieved by using the appropriate Stationary Phase Method with Fresnel functions presented here. The calculations are accurate and fast enough to avoid long simulation times, which constitute one of the most significant drawbacks that occur in radio-propagation tools, which often pertain to modern high frequency communication wireless networks. Then the scattering of EM waves from building walls in the actual 3D radio coverage problem in urban outdoor environment can be formulated through the method presented in this paper. Other numerical and efficient methods for the same scattering problem for a rectangular plate have also been introduced by our research group [3].

The inclusion of Fresnel functions in three dimensional SPM method with analytical results for the calculation of EM wave scattering from rectangular plate geometries has not been documented in literature [4–15] and appears to be very useful for calculating the path loss in urban outdoor environments [16]. In this paper (Section 5), three dimensional SPM-F simulation results are compared to corresponding results obtained in the Near\Fresnel-zone\Far field areas with other methods. These results validate the excellent accuracy of the proposed methodology with standard numerical integration,

3D-SPM [1] calculation and Boundary Integral (BI) — Multilevel Fast Multipole Method (MLFMM) full wave Exact Solution results (ES) [17–23]. 3D-SPM-F method presented here proves to be more accurate and equally fast in computation times when compared to 3D-SPM [1]. Finally, the finite conductivity of the rectangular plate is examined in detail in Appendix D since walls, roads and roofs in the actual 3D radiocoverage problem, which eventually are modeled as segments and plates [2], are highly non-PEC surfaces.

2. DEFINITION OF THE ELECTROMAGNETIC SCATTERING PROBLEM/APPROXIMATIONS AND CALCULATIONS

2.1. Electromagnetic Layout

An electromagnetic wave is considered to be incident in the direction of wave vector $\underline{k}_i$ upon a PEC rectangular plate of negligible thickness, according to the layout in Fig. 1. According to Fig. 1, the plate vertices lie at the intersections of the lines $x = a, b$ and $y = c, d$. A pair of angles, namely θ_i ($\mathrm{T\hat{O}z}$) and φ_i defines the direction of incidence. Assuming that transmitter T lies at a point $z > 0$ far from the scattering plate, our first goal is the calculation of the vector potential $\underline{A}$ at an arbitrary observation point $R(x, y, z)$ with $z > 0$, and subsequently, the calculation of the electric field $\underline{E}$ at the same observation point, which lies in the near, intermediate (Fresnel) or the far (Fraunhofer) field region of the scatterer. The time dependence of the electric field is proportional to the factor $\exp(+j\omega t)$.

In the cases of GSM, UMTS, Wi-Fi or Wi-Max network technologies, the operating frequency is about 1 GHz or higher. At that frequency, scatterers such as buildings are considered to be electrically large, and current density induced on the scatterer may be calculated with good accuracy using the Physical Optics (PO) approximation. Then, by using appropriate three-dimensional Green's function, the vector potential calculation leads us to an integral expression, which is in the form of an amplitude function multiplied by a complex exponential, i.e., the phase function. In this equation, it is possible to apply our proposed SPM-F method in order to calculate the vector potential, and eventually the electric field. This two dimensional scatterer is a necessary prerequisite in order to model propagation in an urban outdoor environment, which consists of three dimensional walls and other scatterers.

2.2. Current Density Calculation Using Physical Optics (PO) Approximation — Vector Potential Calculation — Electric Field Calculation

The well-known current density induced on the surface of the PEC rectangular plate due to an incident plane wave with wavevector $\underline{k}_i$, according to the PO approximation is presented in [2, 4]. Then, by referring to [1] and by applying the PO current density approximation $\underline{J}_s$ on the rectangular plate mentioned above, the vector potential $\underline{A}(x, y, z)$ at an arbitrary observation point $R(x, y, z)$ with $z > 0$ results in the following equation:

$$\begin{aligned}\underline{A}(x,y,z) \;=\; & \frac{-\mu_0}{2\pi\eta}\left[\hat{x}(E_{0\theta}\cos\phi_i - \mathrm{E}_{0\phi}\cos\theta_i\sin\phi_i)\right. \\ & \left.+\hat{y}\left(E_{0\theta}\sin\phi_i + E_{0\phi}\cos\theta_i\cos\phi_i\right)\right] \\ & \cdot \int_{y'=d}^{c}\int_{x'=b}^{a} \frac{e^{jk(x'K+y'L)}e^{-jk\sqrt{(x-x')^2+(y-y')^2+z^2}}}{\sqrt{(x-x')^2+(y-y')^2+z^2}}dx'dy' \quad (1)\end{aligned}$$

where μ_o: magnetic permeability of the vacuum ($\mu_o = 4\pi \cdot 10^{-7}$ H/m); $r = (x, y, z)$: position vector of observation; $r' = (x', y')$: position vector of source current; $\eta = \sqrt{\mu_0/\varepsilon_0}$ = free space impedance, $k = 2\pi/\lambda$ is the wavenumber, and K, L are constants which depend on the angles of incidence (θ_i, φ_i) [4].

In [1], the vector potential $\underline{A}$ of Eq. (1) has already been computed with three different ways, i.e., SPM, standard numerical integration (NI) in two dimensions and exact solution (ES) [17–23]. SPM-F method and results follow in sections below.

The calculation of the scattered electric field $\underline{E}$ follows the calculation of vector potential $\underline{A}$ according to formula (A1).

3. STATIONARY PHASE METHOD WITH FRESNEL FUNCTIONS CALCULATIONS (SPM-F)

The main contribution terms in stationary phase method approximations are presented in Eqs. (2)–(7), below. The core algorithm [1] is now explained in detail and the edge point contribution terms will be changed in order to include the newly introduced higher order approximation terms with Fresnel functions. Initially we calculate asymptotically the definite Double Integral (DI) of the form:

$$I(k) = \int_{d}^{c}\int_{b}^{a} F(x,y)e^{jkf(x,y)}dxdy \quad (2)$$

After the asymptotic calculations [5] take place, the following expression is obtained for Eq. (2):

$$I(k) \sim F(x_s, y_s)\, e^{jkf(x_s,y_s)} \frac{j2\pi\delta}{k\sqrt{|4AB - C^2|}} \tag{3}$$

where the end-points contribution terms are neglected here, and: k: real wavenumber, relatively high; (x_s, y_s): Stationary point of function $f(x, y)$, i.e., the point where the partial derivatives of the phase function $f(x, y)$ with respect to x and y vanish.

For frequency $f = 1\,\text{GHz}$, $k = 2\pi f/c \approx 21\,\text{m}^{-1}$, a value which for the scatterer's maximum dimension under consideration in this paper can be considered relatively high for Stationary Phase Calculations [5]. In other words, for the numerical implementations of Section 5, the electrical length of the rectangular scatterer's maximum dimension (diagonal of the plate) is $kL_{\max} = 40\pi\sqrt{2} \gg 1$.

Phase function $f(x, y)$: Slowly varying, real, non-singular function, independent of k.

Amplitude function $F(x, y)$: non-singular function, may be complex [5], should also be independent of k. In the present work, $F(x, y)$ is a real-valued function.

a, b, c, d: limits of the double integral. Here it should be emphasized that the stationary point must be placed within the surface boundaries, i.e., $b < x_s < a$, $d < y_s < c$.

A, B, C: Constants related to the second derivatives of the phase function $f(x, y)$, according to the definitions:

$$A = \frac{1}{2} f''_{xx}(x_s, y_s) \tag{4}$$

$$B = \frac{1}{2} f''_{yy}(x_s, y_s) \tag{5}$$

$$C = f''_{xy}(x_s, y_s) \tag{6}$$

δ: the value of δ is determined from the relative values of the constants A, B and C:

$$\delta = \begin{cases} +1, & 4AB > C^2, \quad A > 0 \\ -1, & 4AB > C^2, \quad A < 0 \\ -j, & 4AB < C^2 \end{cases} \tag{7}$$

To emphasize a previous statement, Eq. (3) is used only in the case when the stationary point lies between the finite limits of the plate, otherwise the SPM contribution vanishes, under the present considerations.

The SPM calculation term denoted in Eq. (3) is not taking into account the contribution from the finite limits of the plate, (a, b,

c, d). In [6], and for the case of single integral calculations (SI), the term over the interval (a, b) is extended to the indefinite interval $(-\infty, +\infty)$ and correction terms related to the edge contributions a, b are subtracted. The core algorithm of our proposed method is to generalize this method [6] for the case of Double Integrals (DI) by adding edge calculation terms based on the Fresnel function (see Section 3.2, below). In Section 3.1, below, we summarize this method [6] for the case of a Single Integral (SI). Furthermore, in Section 3.2, we apply initially the equations of the single integral to appropriate integrand functions. Afterwards, by defining appropriate new integrand functions, we apply the SPM method regarding the second integration of the double integral, always paying attention to include the second order Fresnel function edge approximation terms. The final result is nine integration terms, eight of which take into account the Fresnel function edge terms, as explained in Section 3.2 below, resulting in a new analytical calculation of the double integral in a novel closed form (to our knowledge not documented to date in the literature [4–15]). This novel form uses nine terms of stationary phase, which contain the total information about the finite limits of the plate, (a, b, c, d). The complexity of the corresponding mathematical expressions (elaborate analytical formulas), and the complicate calculations of Fresnel values lead us to implement analytically this method in a standard MATLAB computational package, both for the case of single and double integral. As it will be explained in Section 6, below, Stationary Phase Method analytical calculations, even with edge calculation terms based on Fresnel functions, are very fast in terms of actual computation time. All relative mathematical formulas are described below.

3.1. SPM-F Single Integral Calculations

In the case of the Single Integral (SI), the procedure for the calculation of the limits' contribution to the integral is presented in [6]. In this case, the SPM integral is defined by:

$$I' = \int_b^a F(x) \cdot \exp(jkf(x)) \cdot dx \tag{8}$$

and it can be written subsequently as:

$$\begin{aligned} I' &= \int_{-\infty}^{+\infty} F(x)\exp(jkf(x))\,dx - \int_{a}^{+\infty} F(x)\exp(jkf(x))\,dx \\ &\quad - \int_{-b}^{+\infty} F(-x)\exp(jkf(-x))\,dx = \int_{-\infty}^{+\infty} F(x)\exp(jkf(x))\,dx \\ &\quad - \int_{a}^{+\infty} F(x)\exp(jkf(x))\,dx - \int_{-b}^{+\infty} FF(x)\exp(jkff(x))\,dx \\ &= I_o - I_a - I_b \end{aligned} \tag{9}$$

where functions FF and ff are defined from equations:

$$FF(x) = F(-x) \tag{10}$$

$$ff(x) = f(-x) \tag{11}$$

I_o term is calculated according to [6] or equivalently according to [5], as:

$$I_o = \sqrt{\frac{2\pi}{k\left|f''(x_o)\right|}}F(x_o)\cdot\exp\left(j\left[kf(x_o)+\frac{\pi}{4}\mathrm{sgn}\left\{f''(x_o)\right\}\right]\right) \tag{12}$$

where x_o denotes the stationary point for which $f'(x_o) = 0$. For the other two terms, higher order approximation terms using Fresnel functions are taken into account:

$$I_q = \varepsilon_q \cdot F(q)\exp\left\{jkf(q) \mp ju_q^2\right\} \times \sqrt{\frac{2}{k\left|\frac{\partial^2 f}{\partial x'^2}\Big|_{x'=q}\right|}}Fr_{\pm}[u_q] \tag{13}$$

where $q = a, b$ and

$$\varepsilon_q = \mathrm{sgn}(q - x_o) \tag{14}$$

$$u_q = \sqrt{\frac{k}{2\left|\frac{\partial^2 f}{\partial x'^2}\Big|_{x'=q}\right|}}\left|\frac{\partial f}{\partial x'}\Big|_{x'=q}\right| \tag{15}$$

$$Fr_{\pm}(u_q) = \int_{u_q}^{\infty}\exp\left(\pm jt^2\right)dt \tag{16}$$

where the combination $(\exp\left\{jkf(q) - ju_q^2\right\},\ Fr_+[u_q])$ is used in Eq. (13) when $\left(\frac{\partial^2 f}{\partial x'^2}\Big|_{x'=q}\right) \geq 0$, and the combination

$(\exp\{jkf(q)+ju_q^2\},\ Fr_-[u_q])$ in the same equation is used when $\left(\left.\frac{\partial^2 f}{\partial x'^2}\right|_{x'=q}\right)<0$. According to notation (see also Section 5 below), second order approximation terms with Fresnel functions are valid when parameters $u_q \leq 3.0$ [6], otherwise simple SPM calculations [1] apply.

Using the above formulas (9), (12), (13)–(16) of Stationary Phase Method with Fresnel functions (SPM-F), we have presented a complete approximate formula for the asymptotic calculation of the Single Integral (SI) using Fresnel functions (SPM-F).

3.2. SPM-F Double Integral Calculations

In this section, we will derive the closed-form analytical formulas for the calculation of the Double Integral [DI, Eq. (2)] according to the newly proposed enhanced analytical SPM-F method†. Our final results will be included in Eqs. (20), (A8), (A9), (24), (29) and (39) below.

Integrals of the form of Eq. (2) are frequently encountered during the procedure of calculating the vector potential $\underline{A}$ in common electromagnetic problems. Assuming an incident plane wave which is scattered by a perfect conducting plate, we calculate the vector potential $\underline{A}$ using SPM-F approximations, and subsequently, the electric field $\underline{E}$ at an arbitrary observation point $R(x,y,z)$. For the calculation of the vector potential, we assume current density distribution according to the Physical Optics (PO) approximation, which is sufficiently accurate for electrically large scatterers (i.e., $kL_{\max} \gg 1$, where $L_{\max}$ is the maximum dimension of the scatterer). This result is important, because it provides a very fast method of calculation, as compared to standard numerical integration techniques. Furthermore, it provides an analytical (instead of numerical) method for the calculation of the scattered electric field. Extending these results, we may obtain an expression for the prediction of path losses in an electromagnetic propagation scenario.

We rewrite Eq. (2) with slightly modified variables so that it complies with the form of Eq. (8) above, as follows:

$$I(k;x,y,z)=\int_{y'=d}^{c}\int_{x'=b}^{a}F\left(x,y,z,x',y'\right)e^{jkf(x,y,z,x',y')}dx'dy' \qquad (17)$$

† An alternative, far more complicated way for calculating Eq. (17) is by using an appropriate combination of rotation and change of variables in the double integral, as described in brief in [6], a method that we intentionally avoided here — see Appendix B.

Equation (17) refers to functions F and f, which are functions of two variables, so we have to calculate a double integral, and the algebraic expressions must be modified properly. Using Eq. (9), Eq. (17) is calculated in two steps, in order to take into account the contribution of all four limits of the plate (a, b, c, d).

The first step is related to the calculation of the inner (single) integral of Eq. (17), and it is described by Eqs. (18), (19) and (A2)–(A4) below:

$$\tilde{I'}_q = \operatorname{sgn}(q - x_o) \cdot F\left(q, y'\right) \exp\left\{jkf\left(q, y'\right) \mp j(u_q(q, y'))^2\right\} \times \sqrt{\frac{2}{k\left|\frac{\partial^2 f}{\partial x'^2}\Big|_{x'=q, y'=y'}\right|}} Fr_{\pm}\left[u_q\left(q, y'\right)\right] \tag{18}$$

$$u_q\left(q, y'\right) = \sqrt{\frac{k}{2\left|\frac{\partial^2 f}{\partial x'^2}\Big|_{x'=q, y'=y'}\right|}} \left|\frac{\partial f}{\partial x'}\Big|_{x'=q, y'=y'}\right| \tag{19}$$

where $q = a, b$ and ($\mp$ and $\pm$) combination varies according to Section 3.1 and $x_o = x_o(y')$ is the curve determined by equating the first partial derivative of the phase function $f(x', y')$ with respect to x' with zero, replacing the variables $x' = x_o$ and $y' = y'$, and solving with respect to x_o as explained in Eq. (A5).

3.3. Area Division Approach

Equation (17) is extended properly, to include calculations involving Eqs. (18), (19), (A2)–(A4). According to our proposed first approach, the domain surrounding the rectangular patch is being divided into four separate regions (regions 1–4, while region 0 corresponds to the whole x-y plane) according to the pattern in Fig. 2.

According to Fig. 2, Eq. (17) may be rewritten as in Eq. (A6) or, equivalently as in Eq. (A7) or (20).

$$I(k; x, y, z) = I_0 - I_1 - I_2 - I_3 - I_4 \tag{20}$$

Term $I[0] = I_0$ is calculated according to Eq. (3), using the notation of Eq. (12) [where Eq. (12) has been written for the Single Integral case] — see also Eq. (A8).

Equations (3) and (A8) are equivalent expressions, in a slightly different form, but leading to the same result.

Regarding the calculation of integral $I[1] = I_1$, this is calculated in the following two steps: First the inner integral (from $x' = a$ to $x' = +\infty$) is calculated according to Eq. (18). Then by defining

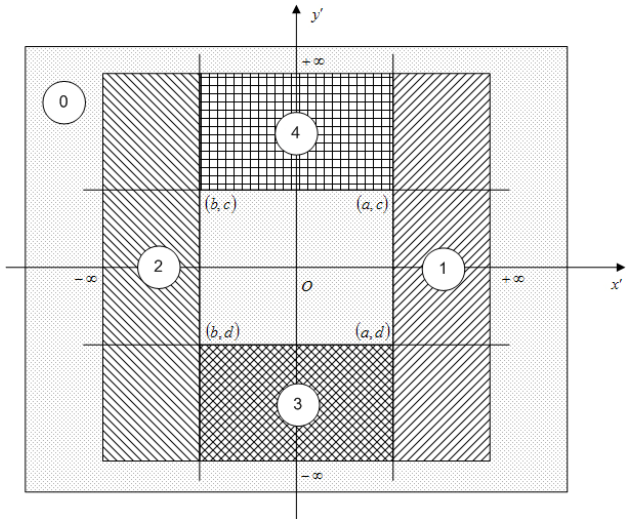

Figure 2. Ranges of integration for the calculation of integral of Eq. (17).

new appropriate amplitude and phase functions (F'_{02} and f'_{02}) by the following equations:

$$F'_{(02)}\left(y'\right)=\mathrm{sgn}\left(a-x_o\right)F\left(a,y'\right)\sqrt{\frac{2}{k\left|\frac{\partial^2 f}{\partial x'^2}\right|_{x'=a,y'=y'}}}Fr_{\pm}\left[u_a\left(y'\right)\right] \quad (21)$$

$$u_a\left(y'\right)=\sqrt{\frac{k}{2\left|\frac{\partial^2 f}{\partial x'^2}\right|_{x'=a,y'=y'}}}\left|\frac{\partial f}{\partial x'}\right|_{x'=a,y'=y'}\left| \quad (22)$$

$$f'_{(02)}\left(y'\right)=f\left(a,y'\right)\mp\frac{\left(\left.\frac{\partial f}{\partial x'}\right|_{x'=a,y'=y'}\right)^2}{2\left|\frac{\partial^2 f}{\partial x'^2}\right|_{x'=a,y'=y'}} \quad (23)$$

the outer integration (for $-\infty < y' < +\infty$) is performed again using the SPM of Eq. (A4). The final result of this procedure is obtained by Eq. (A9), where y_{02} is a modified stationary point defined by Eq. (A10).

In the same way integral $I[2] = I_2$ is calculated. The final result

is:

$$I_2 = \int_{-\infty}^{+\infty}\int_{-\infty}^{x'=b} F\left(x',y'\right)e^{jkf(x',y')}dx'dy' \sim \sqrt{\frac{2\pi}{k\left|\frac{\partial^2 f'_{(03)}}{\partial y'^2}\Big|_{y'=y_{03}}\right|}}F'_{(03)}\left(y_{03}\right)$$
$$\exp\left(j\left[kf'_{(03)}\left(y_{03}\right)+\frac{\pi}{4}sgn\left\{\frac{\partial^2 f'_{(03)}}{\partial y'^2}\Big|_{y'=y_{03}}\right\}\right]\right) \quad (24)$$

where functions F'_{03} and f'_{03} are defined by equations:

$$F'_{(03)}\left(y'\right)=\mathrm{sgn}\left(b-x_o\right)F\left(b,y'\right)\sqrt{\frac{2}{k\left|\frac{\partial^2 f}{\partial x'^2}\Big|_{x'=b,y'=y'}\right|}}Fr_{\pm}\left[u_b\left(y'\right)\right] \quad (25)$$

$$u_b\left(y'\right)=\sqrt{\frac{k}{2\left|\frac{\partial^2 f}{\partial x'^2}\Big|_{x'=b,y'=y'}\right|}}\left|\frac{\partial f}{\partial x'}\Big|_{x'=b,y'=y'}\right| \quad (26)$$

$$f'_{(03)}\left(y'\right)=f\left(b,y'\right)\mp\frac{\left(\frac{\partial f}{\partial x'}\Big|_{x'=b,y'=y'}\right)^2}{2\left|\frac{\partial^2 f}{\partial x'^2}\Big|_{x'=b,y'=y'}\right|} \quad (27)$$

and y_{03} is a modified stationary point defined by:

$$\frac{\partial f'_{(03)}\left(y'\right)}{\partial y'}\Big|_{y'=y_{03}}=0 \quad (28)$$

Regarding the calculation of integral $I[3]=I_3$ in Eqs. (A7), (20), this is also calculated in two steps as follows: First the inner integral (for $b\le x'\le a$) is calculated using the SPM-F formulation through Eqs. (18), (19), (A2)–(A4), and subsequently the outer integration (for $-\infty<y'\le d$) is calculated through Eq. (18). Then the final result is given below Eqs. (29)–(35):

$$I_3 = \int_{-\infty}^{y'=d}\int_{x'=b}^{a} F\left(x',y'\right)e^{jkf(x',y')}dx'dy' = \int_{-\infty}^{y'=d}\left(I'_0-I'_a-I'_b\right)dy'$$
$$= I_{3.1}-I_{3.2}-I_{3.3} \quad (29)$$

where integrals $I[3.1]$, $I[3.2]$ and $I[3.3]$ are calculated as:

$$I_{3.1} = \int_{-\infty}^{y'=d} I'_o dy' = \mathrm{sgn}\,(d-y_{01}) F'_{(01)}(d) \exp\left\{jkf'_{(01)}(d) \mp j(u_d^{(1)}(d))^2\right\} \times \sqrt{\frac{2}{k\left|\frac{\partial^2 f'_{(01)}}{\partial y'^2}\right|_{y'=d}}} Fr_{\pm}\left[u_d^{(1)}(d)\right] \tag{30}$$

$$u_d^{(1)}(d) = \sqrt{\frac{k}{2\left|\frac{\partial^2 f'_{(01)}}{\partial y'^2}\right|_{y'=d}}} \left|\frac{\partial f'_{(01)}}{\partial y'}\right|_{y'=d}\Bigg| \tag{31}$$

$$I_{3.2} = \int_{-\infty}^{y'=d} I'_a dy' = \mathrm{sgn}\,(d-y_{02}) F'_{(02)}(d) \exp\left\{jkf'_{(02)}(d) \mp j(u_d^{(2)}(d))^2\right\} \times \sqrt{\frac{2}{k\left|\frac{\partial^2 f'_{(02)}}{\partial y'^2}\right|_{y'=d}}} Fr_{\pm}\left[u_d^{(2)}(d)\right] \tag{32}$$

$$u_d^{(2)}(d) = \sqrt{\frac{k}{2\left|\frac{\partial^2 f'_{(02)}}{\partial y'^2}\right|_{y'=d}}} \left|\frac{\partial f'_{(02)}}{\partial y'}\right|_{y'=d}\Bigg| \tag{33}$$

$$I_{3.3} = \int_{-\infty}^{y'=d} I'_b dy' = \mathrm{sgn}\,(d-y_{03}) F'_{(03)}(d) \exp\left\{jkf'_{(03)}(d) \mp j(u_d^{(3)}(d))^2\right\} \times \sqrt{\frac{2}{k\left|\frac{\partial^2 f'_{(03)}}{\partial y'^2}\right|_{y'=d}}} Fr_{\pm}\left[u_d^{(3)}(d)\right] \tag{34}$$

$$u_d^{(3)}(d) = \sqrt{\frac{k}{2\left|\frac{\partial^2 f'_{(03)}}{\partial y'^2}\right|_{y'=d}}} \left|\frac{\partial f'_{(03)}}{\partial y'}\right|_{y'=d}\Bigg| \tag{35}$$

where functions F'_{01} and f'_{01} are defined by the following equations:

$$F'_{(01)}\left(y'\right) = \sqrt{\frac{2\pi}{k\left|\frac{\partial^2 f}{\partial x'^2}\Big|_{x'=x_o,y'=y'}\right|}}F\left(x_o,y'\right) \exp\left(j\frac{\pi}{4}\mathrm{sgn}\left\{\frac{\partial^2 f}{\partial x'^2}\Big|_{x'=x_o,y'=y'}\right\}\right) \tag{36}$$

$$f'_{(01)}\left(y'\right) = f\left(x_o,y'\right) \tag{37}$$

y_{01} is a modified stationary point defined by:

$$\left.\frac{\partial f'_{(01)}\left(y'\right)}{\partial y'}\right|_{y'=y_{01}} = 0 \tag{38}$$

and functions F'_{02}, f'_{02}, F'_{03} and f'_{03} have been defined previously in Eqs. (21), (23) and (25), (27).

Finally, integral $I[4] = I_4$ in Eqs. (A7), (20) is calculated in the same way with integral $I[3]$ and the final result is given by Eqs. (39)–(45) below:

$$I_4 = \int_{y'=c}^{+\infty}\int_{x'=b}^{a} F\left(x',y'\right)e^{jkf(x',y')}dx'dy' = \int_{y'=c}^{+\infty}\left(I'_o - I'_a - I'_b\right)dy'$$
$$= I_{4.1} - I_{4.2} - I_{4.3} \tag{39}$$

$$I_{4.1} = \int_{y'=c}^{+\infty} I'_o dy' = \mathrm{sgn}\left(c-y_{01}\right)F'_{(01)}(c)\exp\left\{jkf'_{(01)}(c) \mp j\left(u_c^{(1)}(c)\right)^2\right\} \times \sqrt{\frac{2}{k\left|\frac{\partial^2 f'_{(01)}}{\partial y'^2}\Big|_{y'=c}\right|}}Fr_{\pm}\left[u_c^{(1)}\left(c\right)\right] \tag{40}$$

$$u_c^{(1)}\left(c\right) = \sqrt{\frac{k}{2\left|\frac{\partial^2 f'_{(01)}}{\partial y'^2}\Big|_{y'=c}\right|}}\left|\left.\frac{\partial f'_{(01)}}{\partial y'}\right|_{y'=c}\right| \tag{41}$$

$$I_{4.2} = \int_{y'=c}^{+\infty} I'_a dy' = \operatorname{sgn}(c-y_{02}) F'_{(02)}(c) \exp\left\{jkf'_{(02)}(c) \mp j\left(u_c^{(2)}(c)\right)^2\right\} \times \sqrt{\frac{2}{k\left|\frac{\partial^2 f'_{(02)}}{\partial y'^2}\right|_{y'=c}}} Fr_{\pm}\left[u_c^{(2)}(c)\right] \tag{42}$$

$$u_c^{(2)}(c) = \sqrt{\frac{k}{2\left|\frac{\partial^2 f'_{(02)}}{\partial y'^2}\right|_{y'=c}}} \left|\frac{\partial f'_{(02)}}{\partial y'}\right|_{y'=c}\Bigg| \tag{43}$$

$$I_{4.3} = \int_{y'=c}^{+\infty} I'_b dy' = \operatorname{sgn}(c-y_{03}) F'_{(03)}(c) \exp\left\{jkf'_{(03)}(c) \mp j\left(u_c^{(3)}(c)\right)^2\right\} \times \sqrt{\frac{2}{k\left|\frac{\partial^2 f'_{(03)}}{\partial y'^2}\right|_{y'=c}}} Fr_{\pm}\left[u_c^{(3)}(c)\right] \tag{44}$$

$$u_c^{(3)}(c) = \sqrt{\frac{k}{2\left|\frac{\partial^2 f'_{(03)}}{\partial y'^2}\right|_{y'=c}}} \left|\frac{\partial f'_{(03)}}{\partial y'}\right|_{y'=c}\Bigg| \tag{45}$$

Regarding the above calculations of integral $I(k; x, y, z)$ in Eq. (A7), we note here that the modified stationary points y_{01}, y_{02}, y_{03} and x_0 will be included in the final result, only if $y_{01},\ y_{02},\ y_{03} \in (d, c)$ and $\mathrm{x}_0 \in (b, a)$. In any other case, the contribution regarding these integral terms is zero. Also, note here that the stationary point (x_s, y_s) of Eq. (3) coincides with the stationary point (x_o, y_{01}) of Eqs. (A5), (38).

Before proceeding to analytical calculations, we note that for large angles of scattering parameters u_a, u_b, $u_c^{(1)}$, $u_c^{(2)}$, $u_c^{(3)}$, $u_d^{(1)}$, $u_d^{(2)}$, $u_d^{(3)}$ in Eqs. (19), (22), (26), (31), (33), (35), (41), (43) and (45) are larger than 3.0 (u_a, u_b, $u_c^{(1)}$, $u_c^{(2)}$, $u_c^{(3)}$, $u_d^{(1)}$, $u_d^{(2)}$, $u_d^{(3)} > 3.0$) thus the replacement formulas in Eqs. (18) are not uniform according to [6], and equations without Fresnel functions [1] must be used for best accuracy (i.e., combination formulas). Combination formulas are easy to accomplish with an additional control variable, being able to switch simulation results to appropriate formulation between SPM-F and SPM for large

scattering angles.

A second method of calculation of the double integral of Eq. (26), which differs slightly from the method described above (and which finally is not used in the numerical simulations provided in Section 5 below), is presented in Appendix B. A comparison of these two methods is provided in Appendix C.

4. VECTOR POTENTIAL CALCULATIONS USING SPM

In order to calculate the vector potential $\underline{A}$ from Eq. (1) by using the SPM-F method described in Section 3 above, we first define the amplitude $F(x, y)$ and phase functions $f(x, y)$ by:

$$F(x', y') = \frac{1}{\sqrt{(x - x')^2 + (y - y')^2 + z^2}} \tag{46}$$

$$f(x', y') = x'K + y'L - \sqrt{(x - x')^2 + (y - y')^2 + z^2} \tag{47}$$

Note here that the functions F, f satisfy the appropriate conditions for SPM properties, given above (below Eq. (3)). Subsequently, according to the proposed SPM-F method, in Sections 3.2 and 3.3, the application requires various procedures, such as calculation of the partial derivatives, the solution of complicated systems of equations, computation of additional coefficients and implementation of various computational procedures. All the above are calculated by using the symbolic toolbox of MATLAB computational package.

First, we calculate the stationary point for the function $f(x', y')$ by:

$$\left.\frac{\partial f}{\partial x'}\right|_{\substack{x=x_s \\ y=y_s}} \equiv f'_{x'}(x_s, y_s) = 0 \tag{48}$$

$$\left.\frac{\partial f}{\partial y'}\right|_{\substack{x=x_s \\ y=y_s}} \equiv f'_{y'}(x_s, y_s) = 0 \tag{49}$$

By substituting function $f(x', y')$ from Eq. (47), we obtain the following system of equations:

$$\begin{cases} K + \frac{x - x_s}{\sqrt{(x-x_s)^2 + (y-y_s)^2 + z^2}} = 0 \\ L + \frac{y - y_s}{\sqrt{(x-x_s)^2 + (y-y_s)^2 + z^2}} = 0 \end{cases} \tag{50}$$

The solution of the above system yields the stationary point (x_s, y_s) of function$f(x', y')$. Note that for the EM scattering problem under consideration, one stationary point can exist at maximum,

as expected from physical intuition, which corresponds to specular scattering. The solution is found by using the MATLAB computational package, thus yielding the following result:

$$(x_s, y_s) = \left(x + \frac{K\,|z|}{\sqrt{1-K^2-L^2}}, y + \frac{L\,|z|}{\sqrt{1-K^2-L^2}} \right) \tag{51}$$

Having defined the stationary point (x_s, y_s), we check whether this point is located within the dimensions of the plate. This means both x_s and y_s must lie within (b, a) and (d, c) respectively. We continue the application of the method by calculating the A, B, C parameters, by using Eqs. (4), (5) and (6):

$$A = -\frac{y^2 - 2yy_s + y_s^2 + z^2}{2\left(x^2 - 2xx_s + x_s^2 + y^2 - 2yy_s + y_s^2 + z^2\right)^{\frac{3}{2}}} \tag{52}$$

$$B = -\frac{x^2 - 2xx_s + x_s^2 + z^2}{2\left(x^2 - 2xx_s + x_s^2 + y^2 - 2yy_s + y_s^2 + z^2\right)^{\frac{3}{2}}} \tag{53}$$

$$C = \frac{(x - x_s)(y - y_s)}{\left(x^2 - 2xx_s + x_s^2 + y^2 - 2yy_s + y_s^2 + z^2\right)^{\frac{3}{2}}} \tag{54}$$

Substituting the values of the stationary point (x_s, y_s) from Eq. (51) to Eqs. (46)–(47) we obtain:

$$F(x_s, y_s) = \frac{1}{\sqrt{\left(\frac{K|z|}{\sqrt{1-K^2-L^2}}\right)^2 + \left(\frac{L|z|}{\sqrt{1-K^2-L^2}}\right)^2 + z^2}} \tag{55}$$

$$f(x_s, y_s) = \left(x + \frac{K\,|z|}{\sqrt{1-K^2-L^2}} \right) K + \left(y + \frac{L\,|z|}{\sqrt{1-K^2-L^2}} \right) L - \sqrt{\left(\frac{K\,|z|}{\sqrt{1-K^2-L^2}}\right)^2 + \left(\frac{L\,|z|}{\sqrt{1-K^2-L^2}}\right)^2 + z^2} \tag{56}$$

Subsequently, through the definition of Eqs. (46)–(47), the DI SPM method described in Sections 3.2 and 3.3 above is used to calculate the vector potential $\underline{A}$, Eq. (1), where the contribution from the plate edges (boundaries a, b, c, d) are also taken into account. The DI of the vector potential $\underline{A}$, Eq. (1), is therefore calculated according to the definition of F, f by Eqs. (46)–(47), formula (3), and Eqs. (20)–(45) and (A8)–(A10).

We may also note here that the results of Eqs. (3) and (A8) are completely identical. Also note that Eqs. (A9), (24), (30), (32), (34), (40), (42), (44) refer to the contribution of the vertices (a, b, c, d) of the rectangular plate.

Finally, the two components A_x and A_y of the vector potential $\underline{A}$ are obtained according to Eq. (1) by:

$$A_x = \frac{-\mu_0}{2\pi\eta}\left[E_{0\theta}\cos\phi_i - \mathrm{E}_{0\phi}\cos\theta_i\sin\phi_i\right] F\left(x_s, y_s\right)\, e^{jkf(x_s,y_s)} \frac{j2\pi\delta}{k\sqrt{|4AB-C^2|}} \tag{57}$$

$$A_y = \frac{-\mu_0}{2\pi\eta}\left[E_{0\theta}\sin\phi_i + E_{0\phi}\cos\theta_i\cos\phi_i\right] F\left(x_s, y_s\right)\, e^{jkf(x_s,y_s)} \frac{j2\pi\delta}{k\sqrt{|4AB-C^2|}} \tag{58}$$

Having calculated the vector potential $\underline{A}$, we proceed to calculate the scattered electric field $\underline{E}$ as in [1].

5. NUMERICAL RESULTS USING MATLAB

Regarding the numerical implementation, finally yielding the vector potential and scattered electric field for the geometry of Fig. 1, the procedure is as follows: the vector potential $\underline{A}$ is calculated by Eq. (1), where the corresponding integration is calculated through the methods of Sections 3 and 4.

Subsequently, regarding the calculation of the three components of grad (div$\underline{A}$) in the formulae of the scattered electric field [1], this can be performed in MATLAB environment in two different ways. In the first way, function $A(x, y, z)$ is given in analytical form and the appropriate differentiations are calculated analytically in MATLAB environment. In the second way, the appropriate differentiations for calculating grad (div$\underline{A}$) are performed in MATLAB environment using standard numerical differentiation techniques. We have implemented both these techniques in our simulations and excellent agreement was observed.

Furthermore, in our numerical simulations we compare results based on our proposed 3D analytical SPM-F method with 3D analytical SPM method [1], numerical integration technique using Gaussian quadrature [2] and Finite Element Boundary Integral (FEBI) full-wave exact solution (see Ref's. [17–23]). In the case of the numerical integration technique, a numerical integration tolerance error level of 10^{-6} is specified, which is of satisfactory accuracy and leads to acceptable run-time in our simulations.

With working frequency set equal to 1 GHz, the simulation parameters, according to the geometry of Fig. 1 are provided in Table 1:

Table 1. Double integral simulation parameters.

Symbol	Quantity	Value
λ	Wavelength	0.3 m
r	Observation distance	Near Field area[1], Fresnel area[1], Far Field area[1]
φ_i	Angle of incidence	225°
θ_i	Angle of incidence	45°
φ_s	Observation angle	45°
θ_s	Observation angle	$0^\circ - 90^\circ$
$E_{0\theta}$	Constant related to emitted field (θ_i)	1 V/m
$E_{0\varphi}$	Constant related to emitted field (φ_i)	1 V/m
$a-b$	x axis plate dimension	$20\lambda,\ 40\lambda,\ 60\lambda,\ 80\lambda$
$c-d$	y axis plate dimension	$20\lambda,\ 40\lambda,\ 60\lambda,\ 80\lambda$

[1]As calculated from the corresponding Fresnel and Far Field area distances, given by well known expressions as in Ref. [2].

In Figs. 3, 4 and 5, numerical results are displayed for a plate of dimensions $20\lambda \times 20\lambda$ for the far field, Fresnel zone and near field areas respectively. As expected for all these cases, the maximum value for the main scattering lobe is observed for angle of observation θ_s equal to angle of incidence θ_i. Also we note that in the far field area the number of the side lobes is proportional to the electrical size (kL) of the plate (where k is the wavenumber $k = 2\pi/\lambda$, and $L = a-b = c-d$).

5.1. Far Field Area Results

5.1.1. Far Field Approximation

For the Far Field Area, calculations may be further simplified according to the following approximations:

$$\left|\underline{r} - \underline{r'}\right| = \sqrt{(x-x')^2 + (y-y')^2 + z^2} \cong \sqrt{x^2+y^2+z^2} = r \qquad (59)$$

for the amplitude factor and

$$\left|\underline{r} - \underline{r'}\right| = \sqrt{(x-x')^2 + (y-y')^2 + z^2} \cong r - \frac{xx' + yy'}{r} \qquad (60)$$

for the phase factor.

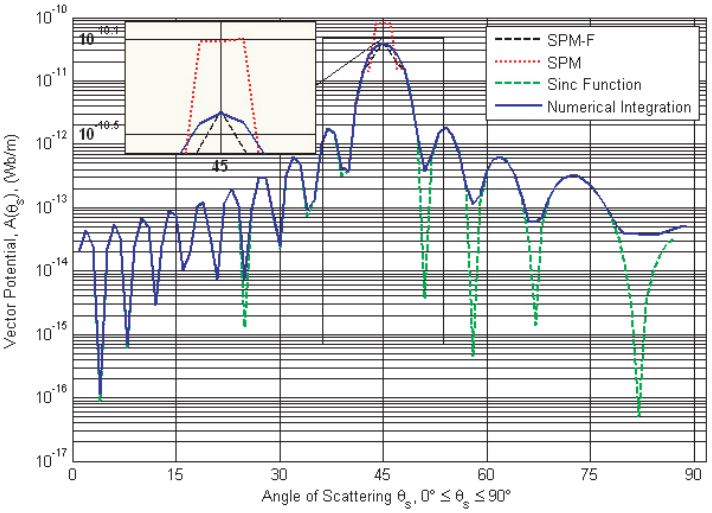

(a) Vector Potential, A (θ_S)

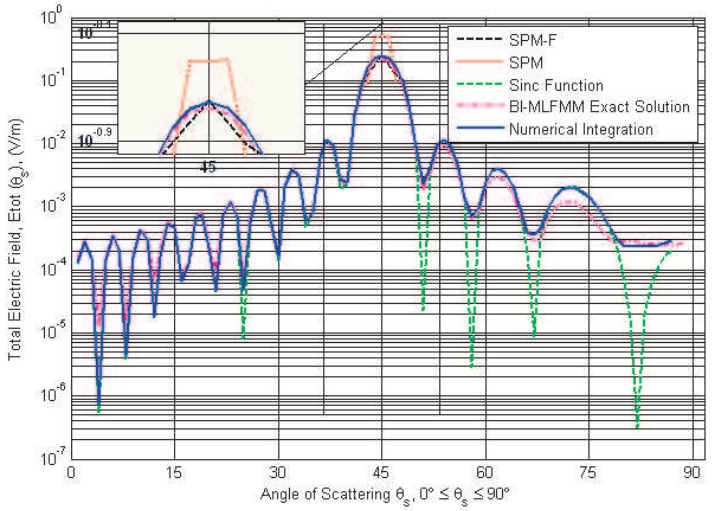

(b) Total Electric Field, Etot (θ_S)

Figure 3. 1 GHz simulation results for plate of dimensions $20\lambda \times 20\lambda$ and observation distance 600 m (Far field area). (a) Magnitude of vector potential $\underline{A}$ as a function of observation angle θ_s. (b) Magnitude of total electric field $\underline{E}$ as a function of observation angle θ_s.

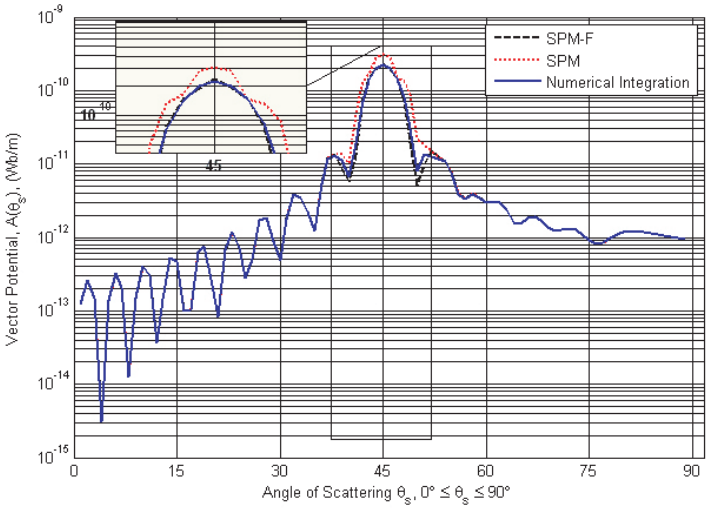

(a) Vector Potential, A (θ_S)

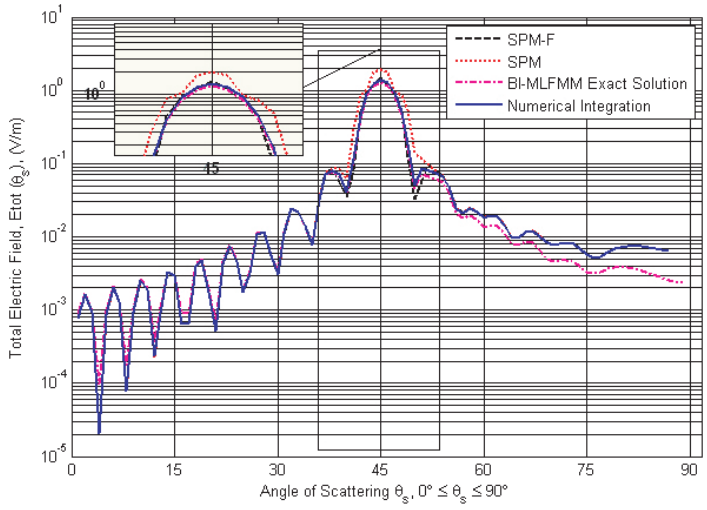

(b) Total Electric Field, Etot (θ_S)

Figure 4. 1 GHz simulation results for plate of dimensions $20\lambda \times 20\lambda$ and observation distance 100 m (Fresnel area). (a) Magnitude of vector potential $\underline{A}$ as a function of observation angle θ_s. (b) Magnitude of total electric field $\underline{E}$ as a function of observation angle θ_s.

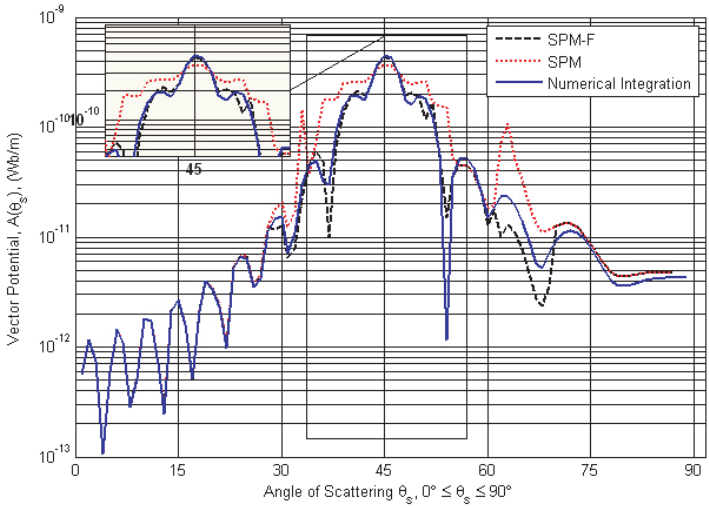

(a) Vector Potential, A (θ_S)

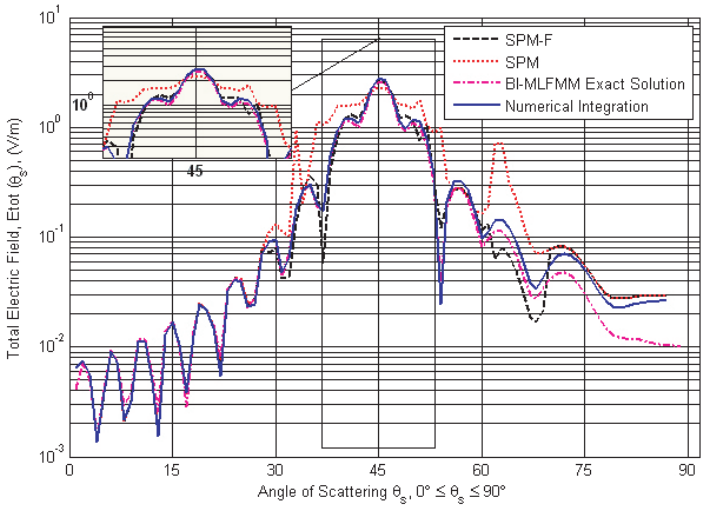

(b) Total Electric Field, Etot (θ_S)

Figure 5. 1 GHz simulation results for plate of dimensions $20\lambda \times 20\lambda$ and observation distance 25 m (Near field area). (a) Magnitude of vector potential $\underline{A}$ as a function of observation angle θ_s. (b) Magnitude of total electric field $\underline{E}$ as a function of observation angle θ_s.

Since variables x and y are calculated from

$$\frac{x}{r} = \sin\vartheta_s \cos\varphi_s \tag{61}$$

$$\frac{y}{r} = \sin\vartheta_s \sin\varphi_s \tag{62}$$

the integral of Eq. (17) is transformed to

$$I \cong \frac{e^{-jkr}}{r} \int_{x'=b}^{a} e^{jkx'(\sin\vartheta_i \cos\varphi_i + \sin\vartheta_s \cos\varphi_s)} dx' \cdot \int_{y'=d}^{c} e^{jky'(\sin\vartheta_i \sin\varphi_i + \sin\vartheta_s \sin\varphi_s)} dy' \tag{63}$$

$$I \cong \frac{e^{-jkr}}{r} (a-b)(c-d) \operatorname{sinc}\left[\left(\frac{k(a-b)}{2}\right)(\sin\vartheta_i \cos\varphi_i + \sin\vartheta_s \cos\varphi_s)\right] \operatorname{sinc}\left[\left(\frac{k(c-d)}{2}\right)(\sin\vartheta_i \sin\varphi_i + \sin\vartheta_s \sin\varphi_s)\right] \tag{64}$$

Furthermore, the vector potential $\underline{A}$, and electric field $\underline{E}$ will be simplified to the following expressions:

$$\underline{A}(x,y,z) = \frac{-\mu_0 (a-b)(c-d)}{2\pi\eta} \frac{e^{-jkr}}{r} \{\hat{x}(E_{0\vartheta} \cos\varphi_i - E_{0\varphi} \cos\vartheta_i \sin\varphi_i) + \hat{y}(E_{0\vartheta} \sin\varphi_i + E_{0\varphi} \cos\vartheta_i \cos\varphi_i)\} \cdot \operatorname{sinc}\left[\left(\frac{k(a-b)}{2}\right)(\sin\vartheta_i \cos\varphi_i + \sin\vartheta_s \cos\varphi_s)\right] \operatorname{sinc}\left[\left(\frac{k(c-d)}{2}\right)(\sin\vartheta_i \sin\varphi_i + \sin\vartheta_s \sin\varphi_s)\right] \tag{65}$$

$$|\underline{E}(x,y,z)| = |-j\omega \underline{A}(x,y,z)| \tag{66}$$

5.1.2. Far Field Numerical Results and Comments

From the above results (Fig. 3), it can be easily concluded that the proposed 3D analytical SPM-F method yields results of excellent accuracy for all angles of observation. Also the errors of respective results in SPM method [1] are significantly reduced from 2–4 dB [1] to a maximum of 0.1–0.2 dB here. Also we note that any errors that exist in SPM-F method are reduced in the case of a larger scatterer, i.e, $80\lambda \times 80\lambda$ scatterer (not shown here), as expected once SPM-F is a high frequency asymptotic method. Finally, an error of about 30 dB, which appears at several observation angles between the standard numerical

integration method and the analytical sinc function result, is explained due to the highly oscillatory behavior of the induced physical optics currents on the surface of the rectangular plate.

5.2. Fresnel Area Results and Comments

In this case (Fig. 4), we observe results of very satisfactory accuracy. Errors of about 2–4 dB [1] were reduced significantly to about 0.1 dB. Any errors will be reduced in the case when the scatterer is electrically larger (not shown here/see comment at Section 5.1.2 above).

5.3. Near Field Area Results and Comments

In the case of near field observations, the results (Fig. 5) are found to be rather accurate, since errors of 15 dB in [1] were reduced to 4–7 dB at maximum here. By physical intuition, we expect a larger numerical error at the near field area, since it appears that for this case the field contribution from only one stationary point and the diffracting edges of the scattering plate is not enough for very accurate calculations. Once again, these errors can be corrected when the scatterer is electrically larger (not shown here/see comment at Section 5.1.2 above).

Comparison graphs in Figs. 3–5 above indicate the improved behavior around the area of the main scattering lobe between the asymptotic results of the SPM-F and SPM [1] methods.

6. RUN-TIME CONSIDERATIONS OF THE PROPOSED ANALYTICAL METHOD

Table 2 below compares the run-time needed for all four methods (SPM-F, SPM [1], Numerical Integration — NI [2] and Exact Solution — ES [17–23]) for the cases of 20λ and 80λ plate scatterers on a standard desktop personal computer with Pentium M 2 GHz processor and 1 GB of RAM memory. ES results of a full-wave exact method [Boundary Integral (BI) — Multilevel Fast Multipole Method (MLFMM)/Exact Solution (ES)] [17–23] simulated on an AMD Athlon XP 2800+ (faster processor) are provided only for the case of 20λ scatterer, since it is meaningless to perform such a task for the case of a 80λ scatterer. As shown in Table 2, Stationary Phase Method with Fresnel functions is much faster than numerical integration and almost equal in computation time to 3D SPM [1]. Moreover, as it is clearly seen below in Table 2, we note that the run-time for the proposed 3D analytical SPM-F method is almost independent of the electrical length of the scatterer, unlike the numerical integration (NI) method

where the run-time increases drastically with the electrical length of the scatterer. Furthermore, for the proposed SPM-F the run-time is

Table 2. Total simulation time for calculations at 90 different scattering angles on a standard desktop PC[1].

	Method	Run-Time (sec)	Numerical Integration to SPM-F calculations run-time ratio
far field	**DI SPM-F 20λ**	**2.98**	10
	DI SPM 20λ	2.91	
	DI NI 20λ	30.26	
	DI ES 20λ	2645	
Fresnel area	**DI SPM-F 20λ**	**3.34**	12
	DI SPM 20λ	3.25	
	DI NI 20λ	40.31	
	DI ES 20λ	2645	
near field	**DI SPM-F 20λ**	4.37	14
	DI SPM 20λ	4.31	
	DI NI 20λ	61.46	
	DI ES 20λ	2645	
far field	**DI SPM-F 80λ**	**2.96**	54
	DI SPM 80λ	2.92	
	DI NI 80λ	161.27	
Fresnel area	**DI SPM-F 80λ**	**3.31**	136
	DI SPM 80λ	3.07	
	DI NI 80λ	449.19	
near field	**DI SPM-F 80λ**	**4.21**	150
	DI SPM 80λ	4.11	
	DI NI 80λ	630.01	

[1]Personal computer with Pentium M 2 GHz processor and 1GB of RAM memory for the cases of 20λ and 80λ scatterers.

almost independent of the region of observation (far field or Fresnel area or near field), while for the numerical integration method the corresponding run-time increases drastically as the observation point moves from the far field to the near field area. Finally, it is ascertained in Table 2 that full-wave exact methods are much slower in actual computer computation time than PO based methods for the electrically large scatterers considered in this paper.

Using the above comparison results, we can easily realize the usefulness of the proposed SPM-F method for the urban outdoor radio-coverage problem mentioned in Section 1 [2]. A first 2D approach [2] to a common radio propagation scenario consists of two rectangular buildings. In this case, the following scattering mechanisms [2] must be calculated: 8 scattering phenomena of first order (3 scattering mechanisms and 5 diffraction mechanisms), and a total of 93 phenomena of second order (31 scattering-diffraction mechanisms, 29 double scattering mechanisms and 33 diffraction-scattering mechanisms). A simple addition leads us to the conclusion that in a typical and simple real world scenario of two buildings, a total of 96 calculations of integrals of Eq. (1) related to scattering phenomena are required. Therefore, for this simple scenario and for one scattering angle of observation the acceleration in our radio coverage simulation tool will be 93 times the acceleration corresponding to that provided above for one single plate. Additionally, after realizing

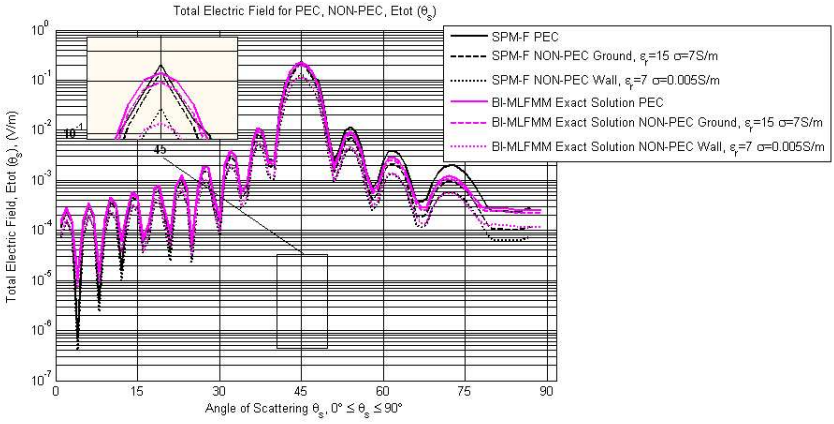

Figure 6. Total scattered electric field comparison results between PEC and non-PEC [ground and wall] rectangular plates of dimensions $20\lambda \times 20\lambda$ in the far field area (600 m), operating frequency 1 GHz.

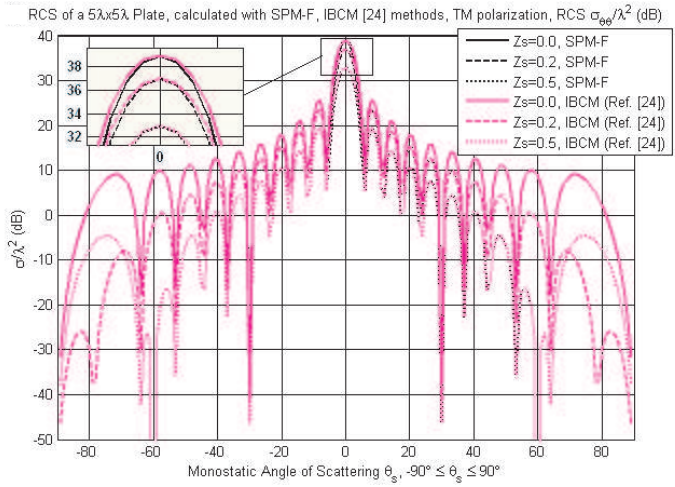

(a)

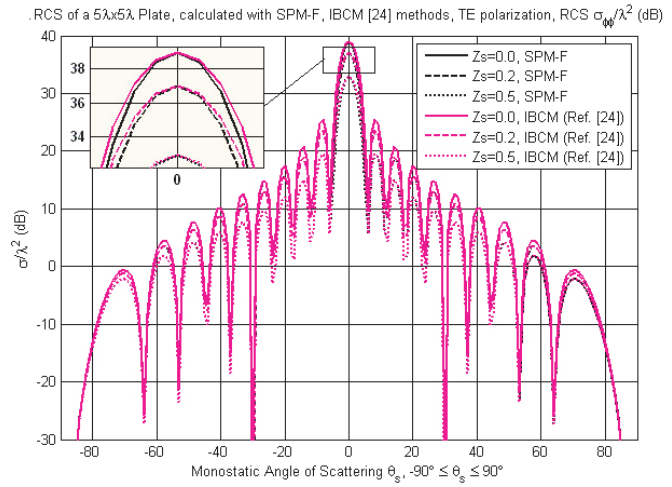

(b)

Figure 7. RCS of a $5\lambda \times 5\lambda$ square plate calculated with SPM-F, IBCM [24] methods, operating frequency 10 GHz. Simulation results for observation distance $r = 600$ m (Far Field area): (a) Radar Cross Section (RCS) $\sigma_{\theta\theta}/\lambda^2$ (dB) (vertical, TM polarization) as a function of monostatic scattering angle θ_s, ($\varphi_s = 0°$). (b) Radar Cross Section (RCS) $\sigma_{\varphi\varphi}/\lambda^2$ (dB) (horizontal, TE polarization) as a function of monostatic scattering angle θ_s, ($\varphi_s = 0°$).

that the above acceleration rates in computation time refer only to one observation point (position and angle), these figures have to be multiplied by the number of resolution cells in the urban scene in order to calculate the total acceleration in computation time for the actual radio coverage problem. Finally, an arduous trial to compare the above methods with full-wave exact solution results (BI-MLFMM FEBI [17–23]), demonstrates faster rates up to 1000 times. In the case of an exact solution with Eventual BIM (pure MoM), a difficult task not performed by our research group, the estimated run-time for the solution of the problem (120,074 unknowns) is approximately 60*3600 sec, whereas the estimated memory required would approximately be equal to 130 GB of RAM.

7. CONCLUSION — FUTURE RESEARCH

In this paper, we presented a novel full 3D analytical method based on the Stationary Phase Method (SPM) and Fresnel functions for the scattering of electromagnetic waves from electrically large conducting rectangular plates. The induced currents on the rectangular plate are calculated through the Physical Optics method and subsequently Stationary Phase Method is used to calculate the contributions from the stationary point within the rectangular plate, as well as the contributions from the diffracting edges of the plate. This method was found to be much more accurate around the main scattering lobe compared to [1] and very fast, compared to standard numerical integration methods [2] and full-wave exact solutions [17–23]. Furthermore, the method proposed here can be used, for example, for calculating the path loss in urban outdoor environments [2, 16]. Finally, the results of [1] were significantly enhanced in all aspects, and SPM-F method adds validity and an asset to the use of Stationary Phase Method techniques for the solution of electromagnetic problems [25, 26].

ACKNOWLEDGMENT

The authors would like to thank Dr. A. Tzoulis for providing the numerical results of Sections 5, 6 and Appendix D based on the exact BI/MLFMM method.

APPENDIX A. BASIC FORMULATION OF THE SPM DOUBLE INTEGRAL CALCULATION

$$\underline{E}(x,y,z) = -j\omega\underline{A} - j\frac{\omega}{k^2}\mathrm{grad}\left(\mathrm{div}\left(\underline{A}\right)\right) \tag{A1}$$

$$\tilde{I}' = \int\limits_{x'=b}^{a} F\left(x',y'\right)e^{jkf(x',y')}dx' \tag{A2}$$

$$\tilde{I}' = \tilde{I}'_0 - \tilde{I}'_a - \tilde{I}'_b \tag{A3}$$

$$\tilde{I}'_0 = \sqrt{\frac{2\pi}{k\left|\left.\frac{\partial^2 f}{\partial x'^2}\right|_{x'=x_o,y'=y'}\right|}}F\left(x_o,y'\right)$$
$$\exp\left(j\left[kf\left(x_o,y'\right)+\frac{\pi}{4}\mathrm{sgn}\left\{\left.\frac{\partial^2 f}{\partial x'^2}\right|_{x'=x_o,y'=y'}\right\}\right]\right) \tag{A4}$$

$$\left.\frac{\partial f\left(x',y'\right)}{\partial x'}\right|_{x'=x_o,y'=y'} = 0 \tag{A5}$$

$$\begin{aligned}
I\left(k;x,y,z\right) &= \int\limits_{y'=d}^{c}\left(\int\limits_{x'=b}^{a}F\left(x',y'\right)e^{jkf(x',y')}dx'\right)dy' \\
&= \int\limits_{-\infty}^{+\infty}\int\limits_{-\infty}^{+\infty}F\left(x',y'\right)e^{jkf(x',y')}dx'dy' \\
&\quad - \int\limits_{-\infty}^{+\infty}\left(\int\limits_{x'=a}^{+\infty}F\left(x',y'\right)e^{jkf(x',y')}dx'\right)dy' \\
&\quad - \int\limits_{-\infty}^{+\infty}\left(\int\limits_{-\infty}^{x'=b}F\left(x',y'\right)e^{jkf(x',y')}dx'\right)dy' \\
&\quad - \int\limits_{-\infty}^{y'=d}\left(\int\limits_{x'=b}^{a}F\left(x',y'\right)e^{jkf(x',y')}dx'\right)dy' \\
&\quad - \int\limits_{y'=c}^{+\infty}\left(\int\limits_{x'=b}^{a}F\left(x',y'\right)e^{jkf(x',y')}dx'\right)dy'
\end{aligned} \tag{A6}$$

$$I(k;x,y,z) = \int_{y'=d}^{c}\int_{x'=b}^{a} F\left(x',y'\right)e^{jkf(x',y')}dx'dy'$$

$$= \int_{-\infty}^{+\infty}\int_{-\infty}^{+\infty} F\left(x',y'\right)e^{jkf(x',y')}dx'dy' - \int_{-\infty}^{+\infty}\int_{x'=a}^{+\infty} F\left(x',y'\right)e^{jkf(x',y')}dx'dy'$$

$$- \int_{-\infty}^{+\infty}\int_{-\infty}^{x'=b} F\left(x',y'\right)e^{jkf(x',y')}dx'dy' - \int_{-\infty}^{y'=d}\int_{x'=b}^{a} F\left(x',y'\right)e^{jkf(x',y')}dx'dy'$$

$$- \int_{y'=c}^{+\infty}\int_{x'=b}^{a} F\left(x',y'\right)e^{jkf(x',y')}dx'dy' \tag{A7}$$

$$I_0 = \int_{-\infty}^{+\infty}\int_{-\infty}^{+\infty} F\left(x',y'\right)e^{jkf(x',y')}dx'dy' = \frac{2\pi F(x_s,y_s)}{k}$$

$$\frac{\exp\left(j\frac{\pi}{4}\left\{\operatorname{sgn}\left(\left.\frac{\partial^2 f}{\partial x'^2}\right|_{x'=x_s,y'=y_s}\right)+\operatorname{sgn}\left(\left.\frac{\partial^2 f}{\partial y'^2}\right|_{x'=x_s,y'=y_s}\right)\right\}\right)}{\sqrt{\left|\left(\left.\frac{\partial^2 f}{\partial x'^2}\right|_{x'=x_s,y'=y_s}\right)\cdot\left(\left.\frac{\partial^2 f}{\partial y'^2}\right|_{x'=x_s,y'=y_s}\right)-\left(\left.\frac{\partial^2 f}{\partial x'\partial y'}\right|_{x'=x_s,y'=y_s}\right)^2\right|}}$$

$$\cdot\exp\left(jkf\left(x_s,y_s\right)\right) \tag{A8}$$

$$I_1 = \int_{-\infty}^{+\infty}\int_{x'=a}^{+\infty} F\left(x',y'\right)e^{jkf(x',y')}dx'dy' \sim \sqrt{\frac{2\pi}{k\left|\left.\frac{\partial^2 f'_{(02)}}{\partial y'^2}\right|_{y'=y_{02}}\right|}}F'_{(02)}\left(y_{02}\right)$$

$$\exp\left(j\left[kf'_{(02)}\left(y_{02}\right)+\frac{\pi}{4}\operatorname{sgn}\left\{\left.\frac{\partial^2 f'_{(02)}}{\partial y'^2}\right|_{y'=y_{02}}\right\}\right]\right) \tag{A9}$$

$$\left.\frac{\partial f'_{(02)}\left(y'\right)}{\partial y'}\right|_{y'=y_{02}} = 0 \tag{A10}$$

APPENDIX B. ALTERNATIVE APPROACH FOR THE CALCULATION OF THE SPM DOUBLE INTEGRAL

Here, we present an approach for the above calculation which is a variant to that proposed in Section 3.3. In this alternative approach the double integral under evaluation, Eq. (A7), namely the integral

$$I\left(k;x,y,z\right)=\int\limits_{y'=d}^{c}\int\limits_{x'=b}^{a}F\left(x',y'\right)e^{jkf(x',y')}dx'dy' \tag{B1}$$

is calculated using SPM in a straightforward way, that is first by integrating over variable x' ($b\leq x'\leq a$) and then by integrating over variable y' ($d\leq y'\leq c$). The inner integration is performed according to Eqs. (18), (19), (A2)–(A4). Subsequently, the outer integration over y' is performed in a way very similar to that described in the previous Section 3.3. Then, the final result of this second approach is presented by the following set of equations, Eqs. (B2)–(B6):

$$I\left(k\right)\sim I_1'-I_2'-I_3' \tag{B2}$$

$$I_1'=I_{01}'-I_c^{(1)}-I_d^{(1)} \tag{B3a}$$

$$I_2'=I_{02}'-I_c^{(2)}-I_d^{(2)} \tag{B3b}$$

$$I_3'=I_{03}'-I_c^{(3)}-I_d^{(3)} \tag{B3c}$$

The terms of Eq. (B3a) are given by:

$$I_{01}'=\sqrt{\frac{2\pi}{k\left|\frac{\partial^2 f_{(01)}'}{\partial y'^2}\right|_{y'=y_{01}}}}F_{(01)}'\left(y_{01}\right)\cdot\exp\left(j\left[kf_{(01)}'\left(y_{01}\right)+\frac{\pi}{4}\mathrm{sgn}\left\{\left.\frac{\partial^2 f_{(01)}'}{\partial y'^2}\right|_{y'=y_{01}}\right\}\right]\right) \tag{B4a}$$

$$I_c^{(1)}=\mathrm{sgn}\left(c-y_{01}\right)F_{(01)}'\left(c\right)\exp\left\{jkf'_{(01)}\left(c\right)\mp j(u_c^{(1)}(c))^2\right\}\times\sqrt{\frac{2}{k\left|\frac{\partial^2 f_{(01)}'}{\partial y'^2}\right|_{y'=c}}}Fr_{\pm}\left[u_c^{(1)}\left(c\right)\right] \tag{B4b}$$

$$I_d^{(1)} = \operatorname{sgn}(d - y_{01})\, F'_{(01)}(d) \exp\left\{ jkf'_{(01)}(d) \mp j\left(u_d^{(1)}(d)\right)^2 \right\} \times \sqrt{\frac{2}{k\left|\frac{\partial^2 f'_{(01)}}{\partial y'^2}\Big|_{y'=d}\right|}}\, Fr_{\pm}\left[u_d^{(1)}(d)\right] \tag{B4c}$$

The terms of Eq. (B3b) are given by the following equations:

$$I'_{02} = \sqrt{\frac{2\pi}{k\left|\frac{\partial^2 f'_{(02)}}{\partial y'^2}\Big|_{y'=y_{02}}\right|}}\, F'_{(02)}(y_{02}) \cdot \exp\left(j\left[kf'_{(02)}(y_{02}) + \frac{\pi}{4}\operatorname{sgn}\left\{ \frac{\partial^2 f'_{(02)}}{\partial y'^2}\Big|_{y'=y_{02}} \right\} \right] \right) \tag{B5a}$$

$$I_c^{(2)} = \operatorname{sgn}(c - y_{02})\, F'_{(02)}(c) \exp\left\{ jkf'_{(02)}(c) \mp j\left(u_c^{(2)}(c)\right)^2 \right\} \times \sqrt{\frac{2}{k\left|\frac{\partial^2 f'_{(02)}}{\partial y'^2}\Big|_{y'=c}\right|}}\, Fr_{\pm}\left[u_c^{(2)}(c)\right] \tag{B5b}$$

$$I_d^{(2)} = \operatorname{sgn}(d - y_{02})\, F'_{(02)}(d) \exp\left\{ jkf'_{(02)}(d) \mp j\left(u_d^{(2)}(d)\right)^2 \right\} \times \sqrt{\frac{2}{k\left|\frac{\partial^2 f'_{(02)}}{\partial y'^2}\Big|_{y'=d}\right|}}\, Fr_{\pm}\left[u_d^{(2)}(d)\right] \tag{B5c}$$

Finally, the terms of Eq. (B3c) are given by the following equations:

$$I'_{03} = \sqrt{\frac{2\pi}{k\left|\frac{\partial^2 f'_{(03)}}{\partial y'^2}\Big|_{y'=y_{03}}\right|}}\, F'_{(03)}(y_{03}) \cdot \exp\left(j\left[kf'_{(03)}(y_{03}) + \frac{\pi}{4}\operatorname{sgn}\left\{ \frac{\partial^2 f'_{(03)}}{\partial y'^2}\Big|_{y'=y_{03}} \right\} \right] \right) \tag{B6a}$$

$$I_c^{(3)} = \operatorname{sgn}(c - y_{03})\, F'_{(03)}(c) \exp\left\{ jkf'_{(03)}(c) \mp j\left(u_c^{(3)}(c)\right)^2 \right\} \times \sqrt{\frac{2}{k\left|\frac{\partial^2 f'_{(03)}}{\partial y'^2}\right|_{y'=c}}}\, Fr_{\pm}\left[u_c^{(3)}(c)\right] \tag{B6b}$$

$$I_d^{(3)} = \operatorname{sgn}(d - y_{03})\, F'_{(03)}(d) \exp\left\{ jkf'_{(03)}(d) \mp j\left(u_d^{(3)}(d)\right)^2 \right\} \times \sqrt{\frac{2}{k\left|\frac{\partial^2 f'_{(03)}}{\partial y'^2}\right|_{y'=d}}}\, Fr_{\pm}\left[u_d^{(3)}(d)\right] \tag{B6c}$$

APPENDIX C. COMPARISON OF THE AREA DIVISION APPROACH (SECTION 3.3) WITH THE DIRECT DOUBLE INTEGRAL CALCULATION APPROACH (APPENDIX B)

Comparing the two methods of calculation mentioned above, we note that Eqs. (B3b)–(B6c) of Appendix B have already appeared during our proposed first approach in Section 3.3 [namely they are Eqs. (A9), (24), (30), (32), (34), (40), (42) and (44)]. Then, the only difference between the two approaches, Section 3.3 and Appendix B respectively, is in the first term of the corresponding representations, namely between Eqs. (A8) and (B4a). Subsequently, after careful consideration of Eqs. (A8) and (B4a), these are found to be exactly the same except for the term: $-\left(\frac{\partial^2 f}{\partial x' \partial y'}\Big|_{x'=x_s, y'=y_s}\right)$ appearing at the denominator of Eq. (A8) [and not appearing at all at the denominator of Eq. (B4a)]. For this reason the first approach (Section 3.3) is considered of higher accuracy than the second approach (Appendix B), due to the fact that it does not ignore the mixed second derivative of the phase function $f(x', y')$ mentioned just above, when taking the appropriate Taylor expansion according to the SPM [5]. Then, in our numerical simulations of Section 5 above, we would rather implement numerically the first approach (Section 3.3).

APPENDIX D. SCATTERING FROM RECTANGULAR PLATE WITH FINITE CONDUCTIVITY

For non Perfect Electric Conductor (non PEC) rectangular plates, as is the case, for example, for the radio coverage problem in urban outdoor environment examined in [2], the scattered electric field as given in [1] should be multiplied, as a first approximation, with the appropriate Fresnel reflection coefficient. This coefficient depends on the electric characteristics of the surface and the operating frequency, as shown below:

$$R_{\perp}(\theta_i) = \frac{\sin(\theta_i) - \sqrt{\varepsilon_c - \cos^2(\theta_i)}}{\sin(\theta_i) + \sqrt{\varepsilon_c - \cos^2(\theta_i)}} \tag{D1}$$

(Fresnel reflection coefficient for perpendicular polarization)

and

$$R_{||}(\theta_i) = \frac{\varepsilon_c \cdot \sin(\theta_i) - \sqrt{\varepsilon_c - \cos^2(\theta_i)}}{\varepsilon_c \cdot \sin(\theta_i) + \sqrt{\varepsilon_c - \cos^2(\theta_i)}} \tag{D2}$$

(Fresnel reflection coefficient for parallel polarization)

where θ_i is the angle of incidence, ε_c is the complex relative dielectric constant of the rectangular plate $\varepsilon_c = \varepsilon_r - j60\sigma\lambda$, ε_r is its relative permittivity, and σ is its conductivity. The values ε_r, σ are chosen according to the literature [16], namely $\varepsilon_r = 15$, $\sigma = 7\,\mathrm{S/m}$ for the ground and $\varepsilon_r = 7$, $\sigma = 0.005\,\mathrm{S/m}$ for the building walls (roofs are not considered at this point, once both transmitter and receiver in our prediction model [2] are considered to be placed well below rooftop level).

According to these values a comparison diagram for the scattered electric field results is presented in Fig. 6.

As clearly seen from the results, in the far field area both SPM-F and BI-MLFMM [21] methods agree not only for the case of a PEC scatterer (as seen in Fig. 3 above), but also for the case of a non-PEC scatterer (Fig. 6). Some minor errors (less than 0.1 dB) are encountered again in the area of the main scattering lobe, as seen clearly from the zoom window provided at the left top corner of the graph. The minor errors are justified, since SPM-F is only a high frequency approximation. Also, minor differences observed for scattering angles θ_s greater than 60 degrees are explained due to the inaccuracies of the PO currents calculated before applying our SPM-F method in those large scattering angles.

Another approximate approach for the scattering from non-PEC rectangular plates might be implemented through the use of the Impedance Boundary Condition Method (IBCM, [24]), which uses the normalized surface impedance Z_s (defined and chosen according to

Ref. [24]) and yields the results of Fig. 7 for the Radar Cross Section (RCS) of a plate of dimensions $5\lambda \times 5\lambda$ at 10 GHz at the Far Field area.

In Fig. 7, some minor errors (less than 0.05 dB as compared to the SPM-F/BI-MLFMM comparison in Fig. 6) are encountered mainly in the area of the main scattering lobe. These errors are significantly smaller than those shown in Figs. 3–6, due to the fact that the operating frequency of 10 GHz is significantly higher than that of Figs. 3–6 (1 GHz), and SPM-F is by definition a high frequency approximation method.

REFERENCES

1. Moschovitis, C. G., K. T. Karakatselos, E. G. Papkelis, H. T. Anastassiu, I. C. Ouranos, A. Tzoulis, and P. V. Frangos, "Scattering of electromagnetic waves from a rectangular plate using an enhanced stationary phase method approximation," *IEEE Trans. Antennas and Propagat.*, Vol. 58, No. 1, 233–238, Jan. 2010.
2. Papkelis, E. G., I. Psarros, I. C. Ouranos, C. G. Moschovitis, K. T. Karakatselos, E. Vagenas, H. T. Anastassiu, and P. V. Frangos, "A radio coverage prediction model in wireless communication systems based on physical optics and the physical theory of diffraction," *IEEE Antennas and Propagation Magazine*, Vol. 49, No. 2, 156–165, Apr. 2007.
3. Papkelis, E., H. Anastassiu, and P. Frangos, "A time efficient near field scattering method applied to radio-coverage simulation in urban microcellular environments," *IEEE Trans. Antennas and Propagat.*, Vol. 56, No. 10, 3359–3363, Oct. 2008.
4. Jenn, D. C., *Radar and Laser Cross Section Engineering*, 29–33, American Institute of Aeronautics and Astronautics, Inc. Washington, 1995.
5. Balanis, C. A., *Antenna Theory: Analysis and Design*, 922–926, John Wiley & Sons, New York, 1996.
6. Graeme, L. J., *Geometrical Theory of Diffraction for Electromagnetic Waves*, 30–42, 61, 90 and 117–123, UK, IEE, 1976.
7. Knott, E. F., J. F. Shaeffer, and M. T. Tuley, *Radar Cross-section*, 2nd Edition, Artech House, 1993.
8. Sirovich, L., *Techniques of Asymptotic Analysis*, 136–147, New York, Springer, 1971.
9. Borovikov, V. A., *Uniform Stationary Phase Method*, London, UK, IEE, 1994.
10. Jones, D. S. and M. Kline, "Asymptotic expansion of multiple

integrals and the method of stationary phase," *J. Math. Phys.*, Vol. 37, 1–28, 1958.

11. Silver, S., *Microwave Antenna Theory and Design*, 119–122, Mc Graw-Hill, 1949.
12. Stiegel, K. M., et al., "Bistatic RCS of surfaces of revolution," *J. Appl. Phys.*, Vol. 26, 297–305, 1955.
13. Born, M. and E. Wolf, *Principles of Optics*, 750–754, Pergamon Press, 1959.
14. Chako, N., "Asymptotic expansion of double and multiple integrals," *J. Inst. Math. Applic.*, Vol. 27, 372–422, 1965.
15. Bleinstein, N. and R. Handelsman, "Uniform asymptotic expansions of double integrals," *J. Math. Anal. Appl.*, Vol. 27, 434–453, 1969.
16. Kanatas, A. G., I. D. Kountouris, G. B. Kostaras, and P. Constantinou, "A UTD propagation model in urban microcellular environments," *IEEE Transactions on Vehicular Technology*, Vol. 46, No. 1, 185–193, Feb. 1997.
17. Wilton, D. R., S. M. Rao, and A. W. Glisson, "Electromagntic scattering by surfaces of arbitrary shape," *IEEE Trans. Antennas Propagat.*, Vol. 30, No. 3, 409–418, May 1982.
18. Song, J., C.-C. Lu, and W. C. Chew, "Multilevel fast multipole algorithm for electromagnetic scattering by large complex objects," *IEEE Trans. Antennas Propagat.*, Vol. 45, No. 10, 1488–1493, Oct. 1997.
19. Eibert, T. F., "A diagonalized multilevel fast multipole method with spherical harmonics expansion of the k-space integrals," *IEEE Trans. Antennas Propagat.*, Vol. 53, No. 2, 814–817, Feb. 2005.
20. Eibert, T. and V. Hansen, "Calculation of unbounded field problems in free space by a 3D FEM/BEM-hybrid approach," *Journal of Electromagnetic Waves and Applications*, Vol. 10, No. 1, 61–78, Jan. 1996.
21. Tzoulis, A. and T. F. Eibert, "A hybrid FEBI-MLFMM-UTD method for numerical solutions of electromagnetic problems including arbitrarily shaped and electrically large objects," *IEEE Trans. Antennas Propagat.*, Vol. 53, No. 10, 3358–3366, Oct. 2005.
22. Tzoulis, A. and T. F. Eibert, "Efficient electromagnetic near-field computation by the multilevel fast multipole method employing mixed near-field/far-field translations," *IEEE Antennas Wireless Propag. Lett.*, Vol. 4, 449–452, 2005.
23. Tzoulis, A., T. Vaupel, and T. F. Eibert, "Ray optical

electromagnetic far-field scattering computations using planar near-field scanning techniques," *IEEE Trans. Antennas Propagat.*, Vol. 56, No. 2, 461–468, Feb. 2008.

24. Jenn, D. C., *Radar and Laser Cross Section Engineering*, 69–76, 2nd Edition, American Institute of Aeronautics and Astronautics, Inc., Reston, Virginia, 2005.
25. Brelet, Y. and C. Bourlier, "SPM numerical results from an effective surface impedance for a one-dimensional perfectly-conducting rough sea surface," *Progress In Electromagnetics Research*, Vol. 81, 413–436, 2008.
26. Zhang, Y., Y. E. Yang, H. Braunisch, and J. A. Kong, "Electromagnetic wave interaction of conducting object with rough surface by hybrid SPM/MoM technique," *Progress In Electromagnetics Research*, Vol. 22, 315–335, 1999.